Discovery of a Rhombohedral Form of the Li-Exchanged Aluminogermanate Zeolite RHO and Its Pressure-, Temperature-, and Composition-Induced Phase Transitions

Yongjae Lee,[†] Thomas Vogt,*[,†] Joseph A. Hriljac,[‡] and John B. Parise[§]

Physics Department, Brookhaven National Laboratory, Upton, New York 11973-5000, School of Chemical Sciences, The University of Birmingham, Birmingham B15 2TT, U.K., and Geosciences Department, State University of New York, Stony Brook, New York 11794-2100

Received March 11, 2002. Revised Manuscript Received May 7, 2002

The influence of pressure, temperature, and composition on the crystal structure of Li-exchanged zeolite RHO with an aluminogermanate framework was investigated using synchrotron X-ray powder diffraction. At ambient conditions, aluminogermanate RHO adopts either a rhombohedral (*R*3) or cubic (*I*23) symmetry depending on the Li-exchange level. Under hydrostatic conditions mediated by an alcohol and water mixture in a diamond-anvil cell, the rhombohedral 68% Li−AlGe−RHO transforms to a cubic structure near 3 GPa, whereas the cubic 57% Li−AlGe−RHO first transforms to a rhombohedral phase near 0.4 GPa and then back to a cubic structure near 3 GPa. The rhombohedral distortion angle, an order parameter of the low-symmetry structure, increases continuously with pressure while approaching the transition to the cubic form, where it decreases abruptly to the equivalent cubic angle. All of these materials show progressive volume contraction under increasing pressure and the calculated bulk moduli suggests that the rhombohedral phase at intermediate pressures is more compressible than its cubic form at higher pressures. Dehydrated samples of both compositions adopt cubic symmetry at ambient conditions and exhibit normal expansion upon heating. During in situ dehydration of hydrated 68% Li−AlGe−RHO, the rhombohedral angle decreases steadily toward the cubic equivalent value until there is an abrupt volume contraction that starts at 300 K and an accompanying transition to a cubic form near 400 K. The hydrated 57% Li−AlGe−RHO maintains its cubic symmetry during in situ dehydration but displays a similar abrupt volume contraction above 350 K. The inverse pressure−temperature relationship is established as shown by the evolution of the rhombohedral angle and the corresponding cell length under pressure and temperature. The rhombohedral-to-cubic phase transitions including the re-entrant behavior observed in the 57% Li−AlGe−RHO are predicted from a distance least-squares approach to framework minimization.

Introduction

Zeolites are naturally occurring aluminosilicate materials crystallizing in a variety of low-density framework structures constructed from corner-connected (Al,SiO_4) tetrahedra. These units define windows with a narrow size distribution of pores and channels with molecular dimensions.[1] The restricted access to the interior, providing reactant, transition state, and product selectivity, makes these "nanoreactors" valuable selective heterogeneous catalysts and ion exchangers in a number of industrial and environmental applications. The built-in flexibility of the T−O−T angle connecting the tetrahedral units allows these structures to contract and expand in response to thermodynamic variables such as temperature and pressure.[2,3] It is also well-known that many zeolites exhibit framework distortions and different cation distributions upon compositional changes via framework cation substitution, ion exchange, dehydration, or sorption.[2,4,5] Because of its exceptional flexibility, zeolite RHO is particularly sensitive to these parameters and has been the subject of extensive structural investigations.[6,7] For example, cadmium ions in aluminosilicate RHO move ca. 5 Å

* To whom correspondence should be addressed. E-mail: tvogt@bnl.gov.
[†] Brookhaven National Laboratory.
[‡] The University of Birmingham.
[§] State University of New York.

(1) Breck, D. W. *Zeolite Molecular Sieves*; Krieger: Malabar, FL, 1984.
(2) Corbin, D. R.; Abrams, L.; Jones, G. A.; Eddy, M. M.; Harrison, W. T. A.; Stucky, G. D.; Cox, D. E. *J. Am. Chem. Soc.* **1990**, *112*, 4821.
(3) Lee, Y.; Hriljac, J. A.; Vogt, T.; Parise, J. B.; Edmondson, M. J.; Anderson, P. A.; Corbin, D. R.; Nagai, T. *J. Am. Chem. Soc.* **2001**, *123*, 8418.
(4) Lee, Y.; Kim, S. J.; Parise, J. B. *Microporous Mesoporous Mater.* **2000**, *34*, 255.
(5) Grey, C. P.; Poshni, F. I.; Gualtieri, A. F.; Norby, P.; Hanson, J. C.; Corbin, D. R. *J. Am. Chem. Soc.* **1997**, *119*, 1981.
(6) Bieniok, A.; Baur, W. H. *J. Solid State Chem.* **1991**, *90*, 173.

10.1021/cm020257r CCC: $22.00
Published on Web 07/25/2002

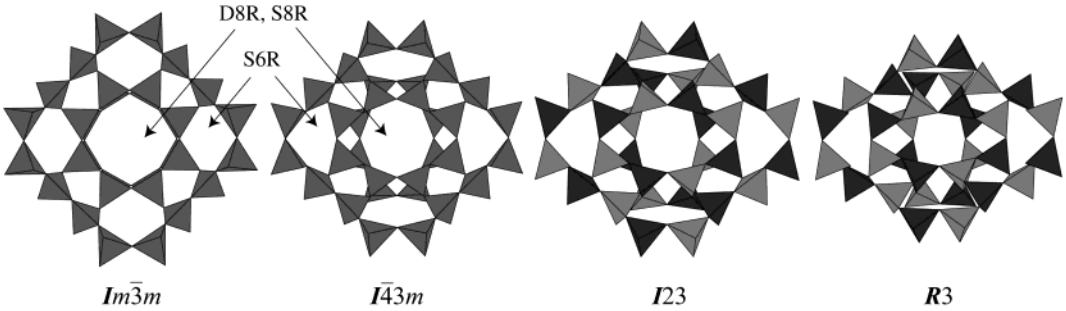

Figure 1. Polyhedral representations of the RHO framework showing deformations in $Im\bar{3}m$, $I\bar{4}3m$, $I23$, and $R3$. D8R building units are shown in the middle and S6Rs at the corners. Al and Si atoms are disordered over the framework T sites in $Im\bar{3}m$ and $I\bar{4}3m$, whereas the Al (light) and Ge (dark) tetrahedra are ordered in $I23$ and $R3$ frameworks. Nonframework cations and water molecules are omitted for clarity.

upon loss of coordinating waters, opening access to the pores, whereas lead ions migrate to different sites and block the access to the pores.[8,9] Recent high-pressure studies on various cation forms of aluminosilicate RHO show cation-dependent phase transition behavior between centric and acentric structures.[3] Because substitution of the framework Si with Ge induces changes in both the framework and nonframework cation distributions,[10,11] the pressure- and temperature-dependent structural changes are expected to be different from those observed in the aluminosilicate materials.

The RHO topology is composed of a body-centered-cubic arrangement of truncated cubooctahedra or α cages linked via double 8 rings of corner-connected tetrahedra. Three sites with unique coordination environments can accommodate the nonframework cations: near the face of a double 8 ring but displaced into the α cage (S8R), in the center of the double 8 ring (D8R), and near the face of a single 6 ring (S6R) (Figure 1). Water molecules are absorbed both in the α cages and in the D8R building units. Depending upon the unit cell composition, which includes hydration level, temperature, and pressure, RHO can adopt a centric $Im\bar{3}m$ or an acentric $I\bar{4}3m$ symmetry when the framework T (tetrahedral) atoms are distributed randomly over the T sites in aluminosilicate frameworks or an acentric $I23$ symmetry when the framework T atoms are ordered in aluminogermanate, beryllophosphate, or berylloarsenate frameworks.[12,13] Although rigid unit mode calculations predict the existence of the $Im\bar{3}$ phase[14] for the disordered form, and consideration of the equitranslation subgroups suggests a number of T-site ordered rhombohedral and orthorhombic structures consistent with the connectivity of the RHO framework, to date none of these are reported. We have investigated the high pressure behavior of (disordered) aluminosilicate RHO and have not found evidence for the $Im\bar{3}$ phase.[3]

To provide a comparison to the high-pressure structural changes observed in aluminosilicate RHOs and to increase the understanding of their comparative crystal chemistry, we have chosen to investigate Li-exchanged aluminogermanate RHO as a function of pressure, temperature, and Li content. Previous neutron diffraction studies on dehydrated Li−AlGe−RHO showed that this material is cubic ($I23$) at ambient conditions with the Al and Ge ordered over the available T sites.[11] Careful examinations of other Li-exchanged samples revealed subtle splittings in their powder X-ray diffraction patterns recorded using a laboratory diffractometer. Using high-resolution synchrotron X-ray diffraction, we have confirmed that these splittings are explained by a rhombohedral distortion of the AlGe−RHO frameworks which have higher nonframework Li contents than the ones used in the neutron diffraction studies. Both cubic and rhombohedral materials were subjected to in situ high-pressure and variable-temperature synchrotron X-ray powder diffraction studies using a diamond-anvil cell (DAC) and a modified He Displex, respectively.

Experimental Section

Synthesis and Li Exchange. The starting material, NaCs−AlGe−RHO, was synthesized from a gel mixture with composition Cs_2O:Na_2O:GeO_2:Al_2O_3:H_2O = 0.7:2.3:2:1:70 according to the procedure reported by Johnson et al.[10] The synthesis yields a material with an approximate composition of $Na_{16}Cs_8Al_{24}Ge_{24}O_{96}{\cdot}nH_2O$. The Li form of AlGe−RHO was prepared by standard ion-exchange procedures. A dried sample was exchanged five times (1 h/cycle) in a 2 M aqueous LiCl (10 mL/g) solution at 60 °C. An ICP chemical analysis (DuPont Co.) gave a chemical composition of $Li_{13.9}Cs_{5.2}Na_{0.2}Al_{24.4}Ge_{23.6}O_{96}{\cdot}nH_2O$. The Cs content is likely to be underestimated given the intrinsic difficulty in analyzing this element with ICP; the other contents should be accurate to within ca. 5%. The structures of the as-synthesized and the five-times Li-exchanged AlGe−RHO's are reported in a cubic space group ($I23$) by Johnson et al.[11] A second set of Li exchanges was performed using eight exchange cycles. Unlike the five-times Li-exchanged sample, the powder diffraction pattern of the eight-times Li-exchanged sample showed peak splitting, and an ICP/FLAA chemical analysis (Galbraith Lab) of this material showed a higher Li content and a unit cell composition of $Li_{16.3}Cs_{7.0}Na_{0.2}Al_{24}Ge_{24}O_{96}{\cdot}nH_2O$. The

(7) Fischer, R. X.; Baur, W. H.; Shannon, R. D.; Staley, R. H.; Abrams, L.; Vega, A. J.; Jorgensen, J. D. *Acta Crystallogr.* **1988**, *B44*, 321.
(8) Parise, J. B.; Xing, L.; Corbin, D. R. *J. Chem. Soc., Chem. Commun.* **1991**, *3*, 162.
(9) Lee, Y.; Reisner, B. A.; Hanson, J. C.; Jones, G. A.; Parise, J. B.; Corbin, D. R.; Toby, B. H.; Freitag, A.; Larese, J. Z.; Kahlenberg, V. *J. Phys. Chem.* **2001**, *B105*, 7188.
(10) Johnson, G. M.; Tripathi, A.; Parise, J. B. *Microporous Mesoporous Mater.* **1999**, *28*, 139.
(11) Johnson, G. M.; Reisner, B. A.; Tripathi, A.; Corbin, D. R.; Toby, B. H.; Parise, J. B. *Chem. Mater.* **1999**, *11*, 2780.
(12) Parise, J. B.; Gier, T. E.; Corbin, D. R.; Cox, D. E. *J. Phys. Chem.* **1984**, *88*, 1635.
(13) Nenoff, T. M.; Parise, J. B.; Jones, G. A.; Galya, L. G.; Corbin, D. R.; Stucky, G. D. *J. Phys. Chem.* **1996**, *100*, 14256.
(14) Bieniok, A.; Hammond, K. D. *Microporous Mesoporous Mater.* **1998**, *25*, 193.

two Li-exchanged AlGe−RHO samples, labeled as 57% Li−AlGe−RHO and 68% Li−AlGe−RHO (errors on Li content ≈ 3%), were used for the variable-temperature and -pressure experiments using synchrotron X-ray powder diffraction.

In Situ Synchrotron X-ray Powder Diffraction. Prior to performing the high-pressure and variable-temperature experiments using synchrotron radiation, experimenters are required to complete beamline-specific and laser safety trainings as well as standard laboratory training.

High-pressure experiments were performed using a diamond-anvil cell (DAC) at beamline X7A of the National Synchrotron Light Source (NSLS) at Brookhaven National Laboratory (BNL). The primary white beam from the bending magnet is focused in the horizontal plane by a triangular, asymmetrically cut Si(220) monochromator bent to a cylindrical curvature by applying a load to the crystal tip, resulting in a microfocused (∼200 μm) monochromatic beam of $\lambda \approx 0.7$ Å.[15] A tungsten wire crosshair was positioned at the center of the goniometer circle, and subsequently the position of the incident beam was adjusted to the crosshair. A gas-proportional position-sensitive detector (PSD)[16] gating on the Kr-escape peak was stepped in 0.25° intervals over the angular range of 3−24° 2θ with counting times of 100−180 s/step. The wavelength of the incident beam (0.7054(1) Å), PSD zero channel, and PSD degrees/channel were determined from a CeO_2 standard (SRM 674).

Powdered samples of the 57% Li−AlGe−RHO and 68% Li−AlGe−RHO were, in turn, loaded into the DAC at ambient pressure and room temperature along with a few small ruby chips. The DAC is based on a modified Merrill−Bassett design[17] and uses two diamonds with 0.5 mm diameter culets on tungsten−carbide supports. The X-rays are admitted by a 0.5 mm diameter circular aperture, and the exit beam leaves via a 0.5 × 3.0 mm rectangular tapered slit, oriented perpendicular to the horizontal plane of the diffractometer. The sample chamber is provided by a 200 or 350 μm hole formed in the center of a 300 μm thick stainless steel gasket, pre-indented to 100 μm thickness before drilling. A mixture of 16:3:1 by volume of methanol/ethanol/water was used as a pressure transmission fluid, which is known to remain hydrostatic up to ∼10 GPa.[18] The pressure at the sample was measured by detecting the shift in the R1 emission line of the included ruby chips.[19] No evidence of nonhydrostatic conditions or pressure anisotropy was detected during our experiments, and the instrumental errors on the pressure measurements ranged between 0.05 and 0.1 GPa. Typically, the sample was equilibrated for about 15 min at each measured pressure prior to data collection. The DAC was then placed on the second axis of the diffractometer, and the sample position was adjusted using the precentered microscope. After the diffraction data measurement, the sample pressure was raised in 0.5−1.0 GPa increments before subsequent data measurements up to a final pressure of 5 GPa. Several pressure points were chosen for diffraction data measurements during pressure release. There was no evidence of stress-induced peak broadening or pressure-driven amorphization, and the recovered sample maintained its original white color and crystallinity.

To compare the structural responses of hydrated and dehydrated materials as a function of temperature, two sets of samples were prepared from each Li−AlGe−RHO sample for the in situ X-ray diffraction studies. The first set was prepared by simply loading each hydrated powder sample at ambient conditions into a 0.3 mm glass capillary. The capillaries were cut to expose both ends for ease of in situ dehydration. The second set was prepared by dehydrating each powder sample in a 0.3 mm quartz capillary under vacuum (∼2 × 10^{-3} Torr). A heating rate of 1 °C/min was used up to 400 °C where it was held for 2 h. The samples were then cooled to room temperature and sealed using a propane/oxygen microtorch. Each capillary sample was used for variable-temperature X-ray diffraction measurements at beamline X7A of the NSLS.

A monochromatic beam was obtained using a channel-cut Si(111) monochromator, and the wavelength of 0.7023(1) Å was calibrated using a CeO_2 standard. The capillary sample was mounted on the second axis of the diffractometer inside a closed-cycle He cryostat, which operates under vacuum and has an absolute temperature accuracy of 5 K and a stability of better than 0.1 K. Diffraction data were measured from 20 K using a PSD stepped in 0.25° intervals over the angular range of 7−37° 2θ with counting times of 60 s/step. The sample temperature was then increased by 50 K intervals up to 550 K for subsequent data measurements. The capillary was rocked by 5° during data collection in order to obtain better powder averaging.

Unit cell parameters were determined by whole-pattern fitting using the variable pressure and temperature data and the LeBail method. The diffraction peaks were modeled by varying only a half-width parameter in the pseudo-Voigt profile function. Using the pressure data, bulk moduli were calculated by fitting the Murnaghan equation of state to the normalized volumes [$V/V_0 = (1 + B'P/B_0)^{-1/B'}$, where $B' = (\partial B/\partial P)_{P=0} = 4$].[20]

Framework Modeling. The fact that the rhombohedrally distorted zeolite RHO has 4 times as many atomic structural parameters than its cubic analogue and, furthermore, that the nonframework Li cations are hard to locate using X-ray data prevented us from deriving structural models using Rietveld refinement. Instead, we have used the measured cell constants and performed distance least-squares (DLS) simulations of the framework to gain some insights into the observed phase transitions between the rhombohedral and cubic structure.

DLS. The use of DLS simulations of crystal structures has been discussed by Meier and Villiger[21] as well as

(15) Lemonnier, M.; Fourme, R.; Rosseaux, F.; Kahn, R. *Nucl. Instrum. Methods* **1978**, *152*, 173.
(16) Smith, G. C. *Synchrotron Rad. News* **1991**, *4*, 24.
(17) Merrill, L.; Bassett, W. A. *Rev. Sci. Instrum.* **1974**, *45*, 290.
(18) Hazen, R. M.; Finger, L. W. *Comparative Crystal Chemistry*; John Wiley & Sons: New York, 1982.
(19) Bell, P. M.; Mao, H. K. *Absolute pressure measurements and their comparison with the ruby fluorescence (R1) pressure scale to 1.5 Mbar*. Carnegie Institute Washington Year Book: Washington, DC, 1979; Vol. 78, p 665.
(20) Angel, R. J. Equations of State. In *High-Temperature and High-Pressure Crystal Chemistry*; Hazen, R. M., Downs, R. T., Eds.; The Mineralogical Society of America: Washington, DC, 2000; Vol. 41, p 35.
(21) Meier, W. H.; Villiger, H. *Z. Kristallogr.* **1969**, *129*, 411.

by Baur.[22] In the study of zeolitic structures, these have been used to derive plausible starting models for the refinement of structures with pseudosymmetry,[23] to test the feasibility of trial models for structure solutions,[24] and to predict the phase stability of a particular framework topology.[12] Provided we can determine with confidence more interatomic distances than there are crystallographically independent positional parameters for a particular structure, these distances may be used as observables in a least-squares procedure to predict a crystal structure. The function minimized is

$$x^2 = \sum_{i=1}^{n} w_i^2[D_i(\text{predicted}) - D_i(\text{model})]^2$$

Here, D_i(model) is the distance between two atoms for a given model, D_i(predicted) is the distance predicted on the basis of the observation of a series of related compounds, and w_i are the weights assigned to D_i(predicted). The framework aluminogermanates as well as aluminosilicates form a class of compounds particularly well suited for this type of DLS refinement. Structural studies at various temperatures and pressures have created a database which allows the prediction of interatomic distances in these compounds. Although the weighting scheme to be used in the procedure is still a matter of debate, it is generally agreed that T−O bond lengths should be given higher weights, while O−O and T−T distances should be given lower weights. The framework modeling was performed in both *I*23 and *R*3 (the only rhombohedral subgroup of *I*23) space groups over a wide range of unit cell dimensions covering the observed values from our pressure and temperature experiments (14.00−15.50 Å cubic equivalent lattice parameters). For the rhombohedral framework, a distortion angle at a particular cell dimension was derived from a fit to the experimental data. The discrepancy index *R* of the DLS was used to show the relative stability of a framework at the particular cell dimensions.

$$R = \sum_{i=1}^{n}\{w_i^2[D_i(\text{predicted}) - D_i(\text{model})]^2\}/\sum_{i=1}^{n} w_i^2 D_i(\text{predicted})^2$$

Results

Variable-Pressure Measurements. That the 68% Li-exchanged RHO is rhombohedrally distorted at ambient pressure can be seen from subtle splittings of the non-*h*00 cubic reflections (Figure 2), whereas the 57% Li-exchanged sample exhibits a body-centered-cubic metric as observed from synchrotron X-ray powder diffraction patterns collected using a medium-resolution ($\Delta d/d \approx 10^{-3}$) position-sensitive detector. The rhombohedral distortion of the 68% Li−AlGe−RHO extends upon pressure increase up to 2.32 GPa as can be seen from the pronounced splitting and shifts of the peaks

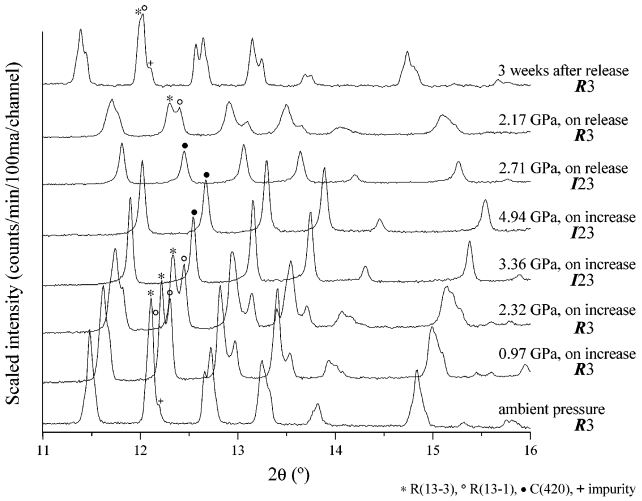

Figure 2. Changes in the synchrotron X-ray powder diffraction patterns observed for 68% Li−AlGe−RHO as a function of pressure.

to higher 2θ (Figure 2). A further increase of pressure results in a transition of the rhombohedral phase to a cubic one, observed at pressures up to 4.94 GPa. When the pressure is gradually released, the high-pressure cubic phase transforms back to the rhombohedral phase, which persists down to ambient pressure (Figure 2). The pressure-induced evolutions of the unit cell parameter and rhombohedral angle of the 68% Li−AlGe−RHO are plotted in Figure 3 with the changes in the normalized volume shown in Figure 4. The volume contraction upon pressure increase is observed in both the rhombohe-dral and cubic phases. In the rhombohedral phase region, the volume contraction is coupled to an increase of the rhombohedral angle, which is an order parameter of this low-symmetry structure and results in a higher bulk modulus of the low-pressure rhombohedral phase compared to the high-pressure high-symmetry cubic form. The phase transition from rhombohedral to cubic near 3 GPa is accompanied by an abrupt lock-in of the rhombohedral distortion angle (Figure 3b). This phase transition is reversed upon pressure release, and the fully recovered sample measured after 3 weeks of pressure release shows slightly larger cell constants (within 3σ) compared to those measured before the pressure cycle starts (Figure 3).

For the 57% Li-exchanged sample, the ambient-pressure cubic structure transforms to a rhombohedral phase near 0.3 GPa (Figure 5a). Upon pressure increase up to 3 GPa, this intermediate-pressure rhombohedral phase shows a progressive volume contraction (Figure 6) and an increasing rhombohedral distortion (Figure 5b) similar to the one observed in the 68% Li−AlGe−RHO sample (Figure 3b). A further increase of pressure above 3 GPa results in a transformation of the rhombohedral phase to a cubic form, which persists up to 4.5 GPa. When the pressure is released, the high-pressure cubic phase transforms back to the rhombohedral phase. Full release of pressure, however, does not recover the original cubic form, and the sample measured after 6 days of pressure release exhibits slightly increased cell constants. The re-entrant phase transition observed in the 57% Li−AlGe−RHO and the retention of the rhombohedral phase upon pressure release are discussed further in a later section.

(22) Baur, W. H. *Phys. Chem. Miner.* **1977**, *2*, 3.
(23) Gramlich, V.; Meier, W. M. *Z. Kristallogr.* **1971**, *133*, 134.
(24) Olson, D. H.; Kokotailo, G. T.; Lawton, S. L.; Meier, W. M. *J. Phys. Chem.* **1981**, *85*, 2238.

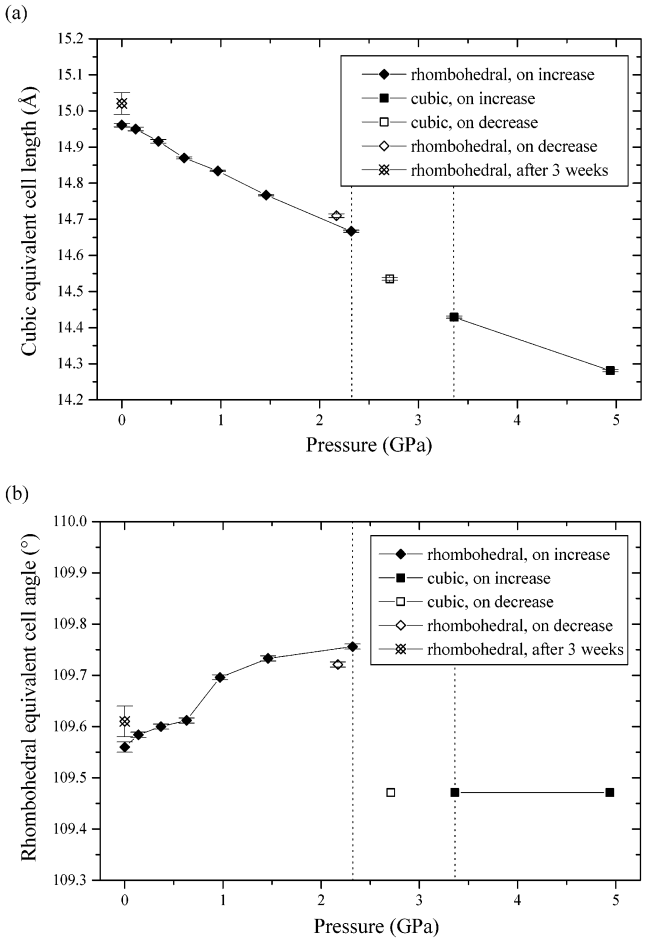

Figure 3. (a) Changes in the cubic equivalent unit cell edge lengths ($a_{\text{rhombohedral}} \times 2/\sqrt{3}$, Å) of 68% Li−AlGe−RHO as a function of pressure. Estimated standard deviations (esd's) are multiplied by 3 at each point. (b) Pressure dependence of the rhombohedral angle of 68% Li−AlGe−RHO. An angle of 109.47° indicates that the metric is cubic.

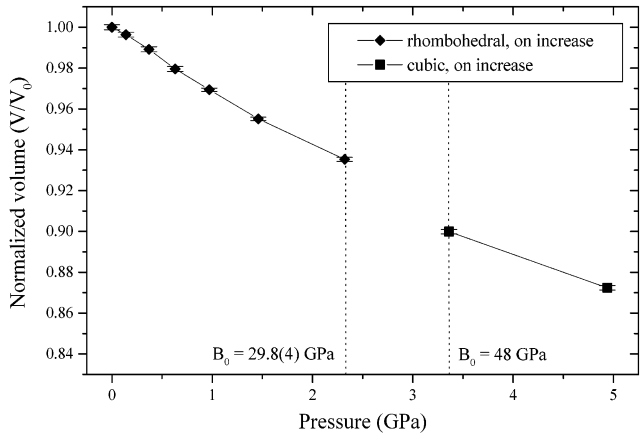

Figure 4. Pressure dependence of the unit cell volume of 68% Li−AlGe−RHO, normalized to its ambient pressure value.

Variable-Temperature Measurements. The temperature-induced changes in the observed powder diffraction patterns of the hydrated 68% Li−AlGe−RHO sample are shown in Figure 7. As the temperature increases from 20 to 300 K, the rhombohedral distortion is reduced progressively with increasing unit cell length, as can be seen from the decreasing splitting and the shift of the sets of peaks to lower 2θ values. Above 350 K, the material starts to lose its zeolitic waters and the structure contracts. During the dehydration between 350 and 400 K, the rhombohedral 68% Li−AlGe−RHO sample transforms to a cubic phase, which contracts further upon dehydration at higher temperatures. In fact, the data collected at 400 and 450 K show the growth of additional contracted/dehydrated cubic phases as shoulder peaks to the right of the major cubic peaks. Above 500 K there exists a single cubic phase. The

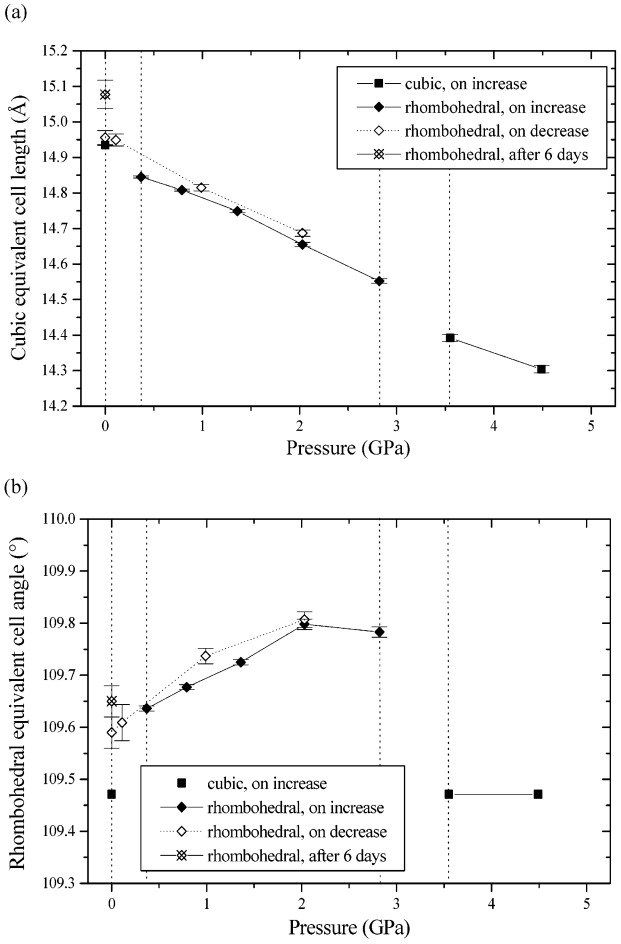

Figure 5. (a) Changes in the cubic equivalent unit cell edge lengths ($a_{\text{rhombohedral}} \times 2/\sqrt{3}$, Å) of 57% Li−AlGe−RHO as a function of pressure. Estimated standard deviations (esd's) are multiplied by 3 at each point. (b) Pressure dependence of the rhombohedral angle of 57% Li−AlGe−RHO. An angle of 109.47° indicates that the metric is cubic.

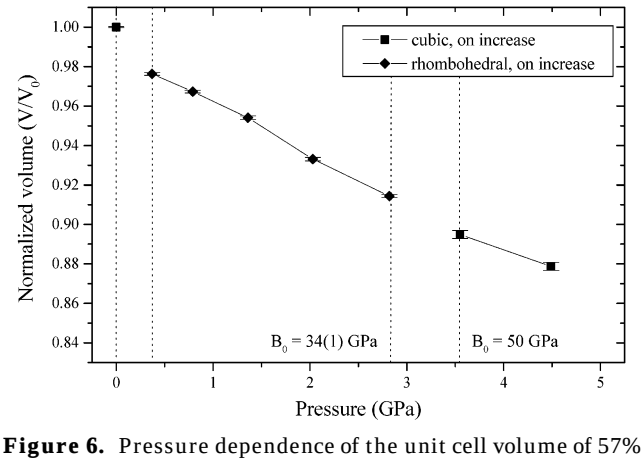

Figure 6. Pressure dependence of the unit cell volume of 57% Li−AlGe−RHO, normalized to its ambient pressure value.

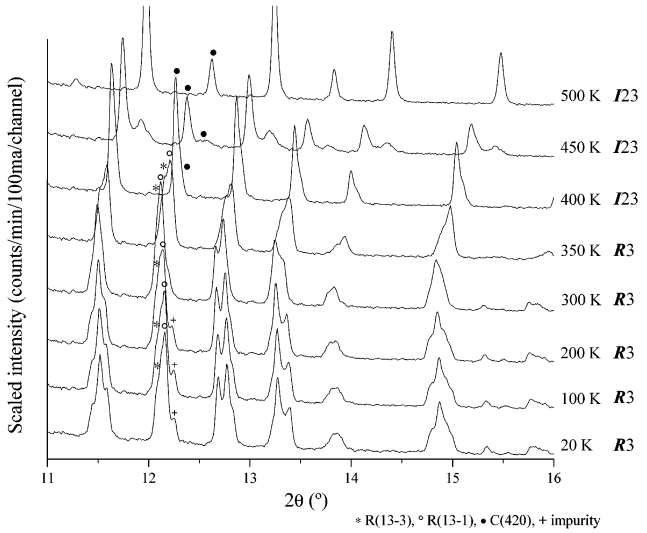

Figure 7. Changes in the synchrotron X-ray powder diffraction patterns observed for the hydrated 68% Li−AlGe−RHO as a function of temperature. Note the presence of two cubic phases in the 400 and 450 K data.

presence of the two cubic phases may arise from either different degrees of dehydration within the crystallites or a temperature gradient in the sample. When the predehydrated 68% Li−AlGe−RHO sample is heated, only a single cubic phase is observed during the temperature range between 20 and 550 K. The temperature-induced evolutions of the unit cell lengths of both hydrated and predehydrated 68% Li−AlGe−RHO samples are plotted in Figure 8a, with the changes in the rhombohedral angle in the hydrated sample shown in Figure 8b. The hydrated rhombohedral phase is shown to be stable above ∼14.7 Å of its equivalent cubic cell lengths, and the dehydration and associated cell contraction result in a transition of the rhombohedral phase to a cubic structure. Unlike the continuous increase in the rhombohedral distortion angle observed in the pressure measurements, the rhombohedral angle converges to the equivalent cubic value as it approaches the cubic phase transition. Possible explanations regarding the different behavior of the order parameter observed in the pressure and temperature measurements are given in the Discussion section. The unit cell volume of the pre-dehydrated sample increases by about 1.1% between 20 and 550 K.

For the hydrated 57% Li-exchanged sample, the ambient-temperature cubic phase persists from 50 K throughout in situ dehydration between 350 and 550 K (Figure 9). Before dehydration, the material shows thermal expansion up to 300 K. During dehydration, an abrupt cell contraction is observed, with the data collected at 500 K showing the growth of a further contracted/dehydrated cubic phase as shoulder peaks to the right of the major cubic peaks (Figure 9), similar to the one observed in the hydrated 68% Li−AlGe−RHO sample (Figure 8a). Based on the re-entrant phase transition behavior of this 57% Li-exchanged material observed during pressure-induced cell contraction, a rhombohedral region would be expected to exist during the dehydration-induced cell contraction. Possible explanations of the observed phase transitions in these Li-exchanged AlGe−RHO materials are given using some framework modeling procedures in the following

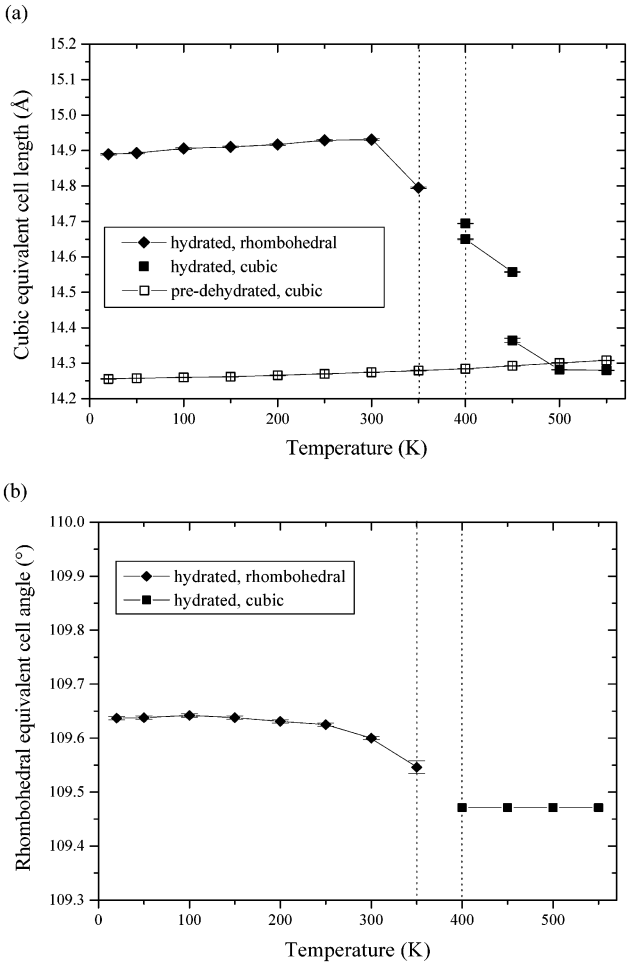

Figure 8. (a) Changes in the cubic equivalent unit cell edge lengths ($a_{\text{rhombohedral}} \times 2/\sqrt{3}$, Å) of the hydrated (closed symbols) and predehydrated (open symbols) 68% Li−AlGe−RHO as a function of temperature. Estimated standard deviations (esd's) are multiplied by 3 at each point. (b) Temperature dependence of the rhombohedral angle of 68% Li−AlGe−RHO. An angle of 109.47° indicates that the metric is cubic.

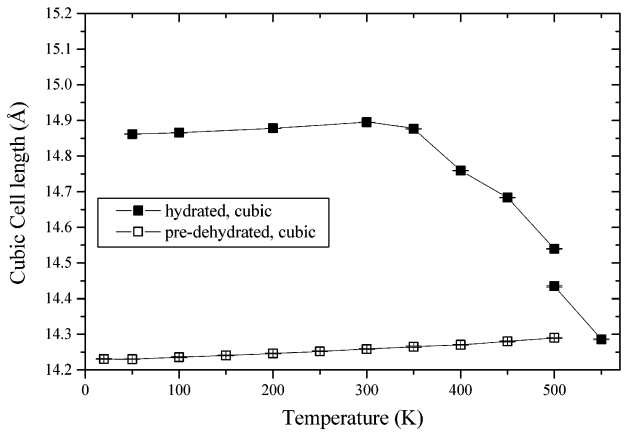

Figure 9. Changes in the cubic unit cell edge lengths (Å) of the hydrated (closed symbols) and predehydrated (open symbols) 57% Li−AlGe−RHO as a function of temperature. Estimated standard deviations (esd's) are multiplied by 3 at each point.

Discussion section. The unit cell volume of the predehydrated 57% Li−AlGe−RHO sample increases by about 1.3% between 20 and 500 K. In both the 57% and 68% Li−AlGe−RHO runs, the cell parameters of the

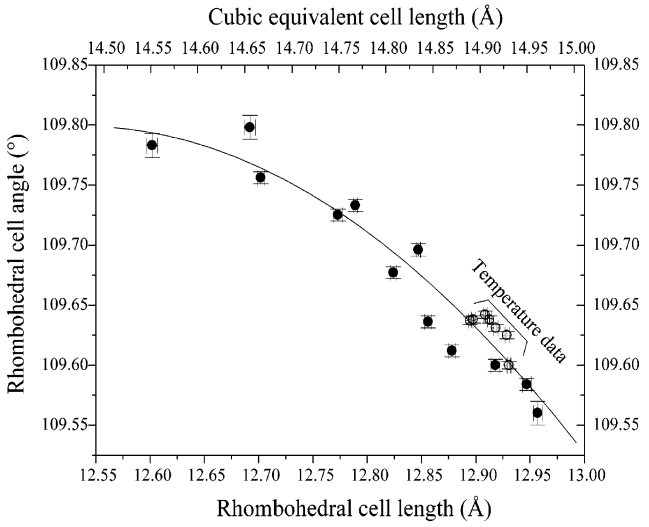

Figure 10. Plot of rhombohedral cell length (*a*, Å) versus rhombohedral angle derived using both the pressure and temperature data (≤300 K). The continuous curve represents a fit by a second-order polynomial.

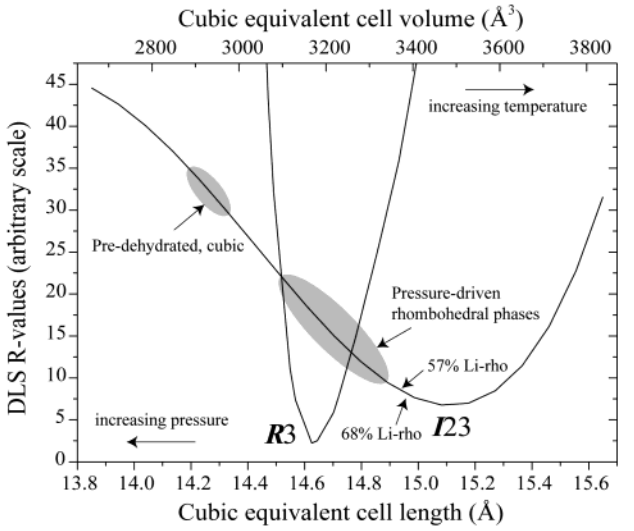

Figure 11. Results of the DLS modeling. Variation of the discrepancy index with equivalent cubic cell dimensions for the framework of zeolite RHO in space groups *I*23 and *R*3 (see text).

hydrated samples at the final dehydration temperatures match closely those of the predehydrated samples, indicating that the in situ dehydration process is finished at around 550 K.

Discussion

Inverse Pressure−Temperature Relationship. In many compounds, the structural changes upon cooling from high temperature are similar to those observed upon compression. This inverse pressure−temperature relationship is regarded to be valid when variable structural parameters such as atomic positions, bond distances and angles, and other distortion parameters show continuous changes over the volume.[18] The variation of the rhombohedral distortion angle is plotted as a function of the rhombohedral cell length using both the pressure and temperature data for the 68% and 57% Li−AlGe−RHO samples (Figure 10). The rhombohedral distortion angle approaches that of the equivalent cubic form (109.47°) as the cell length increases (increasing temperature and decreasing pressure). As the cell length decreases (decreasing temperature and increasing pressure), on the other hand, this distortion angle increases and converges to a maximum around 109.8°. Phase transitions to cubic forms are observed at the left end of this rhombohedral phase stability field through volume contraction induced by either compression or cooling. A continuous change in the rhombohedral distortion angle, an observed structural parameter from both the pressure and temperature measurements, suggests that the inverse relationship of these two thermodynamic variables is confirmed in this class of aluminogermanate framework tetrahedral material, making it possible to predict structural changes with temperature and pressure.

Prediction of the Rhombohedral Stability Region and the Re-entrant Phase Transition. The DLS simulations were performed in the space groups *I*23 and *R*3 using the cubic equivalent lattice parameters in the range between 14.00 and 15.50 Å. *R*3 was the only rhombohedral space group considered because it is the only rhombohedral subgroup of *I*23, and we believe that disordering of the T atoms with pressure to give a different space group is highly unlikely. A weighting scheme of $W(T-O):W(O-O):W(T-T) = 10:2:1$ was used along with ideal interatomic distances of Al−O = 1.74 Å, Ge−O = 1.75 Å, and O−O = 2.84 Å (on Al tetrahedra) and 2.86 Å (on Ge tetrahedra) and O−T−O and T−O−T angles for framework aluminogermanate systems (109.5° and 145°, respectively). The plot of derived DLS *R* values is shown in Figure 11.

The plot for the rhombohedral space group *R*3 is very steep and gives a narrow region (14.5−14.8 Å) where its discrepancy index is lower than the corresponding value in the cubic space group *I*23. The plot for the cubic *I*23 framework, on the other hand, exhibits a broad minimum near 15.1 Å and increases gradually to the left and more steeply to the right. The region of the overlap closely matches the pressure-driven rhombohedral phase region for both 68% and 57% Li−AlGe−RHO samples (see Figures 3a and 5a). Specifically, in the 57% Li−AlGe−RHO, the starting cubic cell was found to transform to a rhombohedral phase between 14.95 and 14.85 Å upon compression and the resulting rhombohedral phase subsequently transforms to a cubic phase upon further compression between 14.55 and 14.40 Å (Figure 5a). The DLS modeling thus predicts this reentrant phase transition between the rhombohedral and cubic structures for the 57% Li−AlGe−RHO sample. The framework modeling, however, does not take into account the compositional difference arising from the nonframework components and the associated framework geometrical changes between the 57% and 68% Li−AlGe−RHO samples. These two samples possess very similar volumes (within 3σ) at ambient pressure, and the reason why the 68% Li−AlGe−RHO is rhombohedral at ambient pressure should, therefore, be addressed considering the details of the framework and nonframework interactions.

The pressure-induced phase transition from a cubic to a rhombohedral phase in the 57% Li−AlGe−RHO sample can be viewed as a first-order transition because there is an energy barrier between the cubic and

rhombohedral phases if one considers the DLS simulation as an approximated one-dimensional energy surface projection. This transition involves a 2.4% volume reduction and shows a discontinuity in the normalized volume variation as a function of pressure (Figure 6). On the other hand, there are no distinct energy minima involved in the rhombohedral-to-cubic transitions occurring at higher pressures in both 68% and 57% Li−AlGe−RHO samples (Figure 11). The region between the high-pressure rhombohedral and cubic phases in the normalized volume variation plots can be better expressed as having a kink between the two phases rather than a discontinuity (Figures 4 and 6). These high-pressure transitions are reversible in both the 57% and 68% Li−AlGe−RHO samples, whereas the rhombohedral-to-cubic transition does not occur in the 57% Li−AlGe−RHO upon full pressure release (Figure 5). The fact that the rhombohedral phase is retained upon the release of pressure can be explained by the fact that the energy minimum associated with this phase is lower than that of the cubic phase at ambient conditions as seen from the DLS simulation (Figure 11). The energy barrier for transformation back to the cubic phase may be overcome by further increasing the cell volume, for example, via increasing its hydration level.

The temperature-driven phase transition from a rhombohedral to a cubic structure in the 68% Li−AlGe−RHO sample can also be rationalized by the DLS modeling. The transition region between 14.8 and 14.7 Å (Figure 8a), however, shows a significant offset by ∼0.2 Å from the value expected from the DLS simulation (Figure 11). Furthermore, a rhombohedral phase region is not observed during dehydration and cell contraction in the 57% Li−AlGe−RHO sample (Figure 9), whereas it is expected to exist according to the DLS modeling (Figure 11). The reason for these discrepancies is attributed to the dehydration and data collection conditions during the in situ heating experiments. Diffraction data measurements were started 10 min after reaching the desired temperature, and the sample was likely under dynamic dehydration during the data collection. Controlling humidity levels and collecting data on the equilibrated samples at temperatures would be required to observe more accurate phase transitions in these samples. On the other hand, the predehydrated samples were measured to have their cubic cell lengths in the range between 14.23 and 14.31 Å (Figures 8a and 9), and this agrees with the DLS expected cubic phase region (Figure 11).

It is important to note that there are apparent compositional changes during the in situ dehydration (above 300 K), whereas there are no indications of chemical changes in the samples during the pressure measurements; a volume expansion would occur if extra water molecules are absorbed into the pores at high pressures.[25] The different behaviors of the rhombohedral distortion angle as a function of pressure and temperature (Figures 3b, 5b, and 8b) may be related to the difference in the composition (hydration level) during each experiment. The dehydration-induced volume contraction between 300 and 400 K relaxes the rhombohedral distortion angle, whereas it increases during the pressure-induced volume contraction. When there are no dehydration-driven compositional changes in the temperature measurement (between 20 and 300 K), the rhombohedral angle shows a continuous decrease with increasing cell constant (Figure 8), which is consistent with the trend seen in the pressure measurements.

Conclusions

The rhombohedral distortion of the RHO topology was observed for the first time in Li-exchanged aluminogermanates. The phase changes upon an increase in pressure and upon a decrease in temperature appear to mirror one another, suggesting that the unit cell volume is the major factor driving these transitions. This is further rationalized using DLS modeling, which predicts the re-entrant phase transition from cubic to rhombohedral and back to the cubic form as the unit cell volume is continuously decreased. The agreement between the observed and modeled phase stability region suggests that this method can be used to predict the existence of the rhombohedral phase in other RHO frameworks such as the beryllophosphates and beryllloarsenates and its transitions at nonambient conditions. Differences in the phase transition behavior for different Li compositions, however, indicate that the volume relationship may not explain all of the behavior observed and that the distribution of nonframework cations may play a significant role. Neutron diffraction studies are in progress to detail the distribution of the nonframework cations in the rhombohedral phase and their pressure- and temperature-dependent rearrangements.

Acknowledgment. This work was supported by an LDRD from BNL (Pressure in Nanopores). J.A.H. acknowledges support from the Royal Society, and J.B.P. appreciates grants from the ACS-PRF and NSF (DMR-0095633). Geoffrey Johnson of Engelhard is acknowledged for the synthesis and ion exchange of the AlGe−RHO samples. Research carried out in part at the NSLS at BNL is supported by the U.S. DOE (DE-Ac02-98CH10886 for beamline X7A). We gratefully acknowledge the Geophysical Laboratory of the Carnegie Institute for access to their ruby laser system at beamline X17C.

CM020257R

(25) Lee, Y.; Hriljac, J. A.; Vogt, T.; Parise, J. B.; Artioli, G. *J. Am. Chem. Soc.* **2001**, *123*, 12732.